energies

MDPI

Article

Towards a Low-Cost Modelling System for Optimising the Layout of Tidal Turbine Arrays

Stephen Nash [1,2,*], Agnieszka I. Olbert [1,2,†] and Michael Hartnett [1,2,†]

Received: 28 September 2015; Accepted: 16 November 2015; Published: 30 November 2015
Academic Editor: John Ringwood

1 College of Engineering & Informatics, National University of Ireland, Galway, University Road, Galway, Ireland; indiana.olbert@nuigalway.ie (A.I.O.); michael.hartnett@nuigalway.ie (M.H.)
2 Marine Renewable Energy Ireland (MaREI), National University of Ireland, University Road, Galway, Ireland
* Correspondence: stephen.nash@nuigalway.ie; Tel.: +353-91-524411
† These authors contributed equally to this work.

Abstract: In the long-term, tidal turbines will most likely be deployed in farms/arrays where energy extraction by one turbine may significantly affect the energy available to another turbine. Given the prohibitive cost of experimental and/or field investigations of such turbine interactions, numerical models can play a significant role in determining the optimum layout of tidal turbine arrays with respect to energy capture. In the present research, a low-cost modelling solution for optimising turbine array layouts is presented and assessed. Nesting is used in a far-field model to telescope spatial resolution down to the scale of the turbines within the turbine array, allowing simulation of the interactions between adjacent turbines as well as the hydrodynamic impacts of individual turbines. The turbines are incorporated as momentum sinks. The results show that the model can compute turbine wakes with similar far-field spatial extents and velocity deficits to those measured in published experimental studies. The results show that optimum spacings for multi-row arrays with regard to power yield are 3–4 rotor diameters (RD) across-stream and 1–4 RD along-stream, and that turbines in downstream rows should be staggered to avoid wake effects of upstream turbines and to make use of the accelerated flows induced by adjacent upstream turbines.

Keywords: tidal turbines; modelling; hydro-environmental impacts; power output; optimising array layout

1. Introduction

Turbines placed in a fluid flow will alter the prevailing hydrodynamics. An area of reduced velocity, the wake, is created behind a turbine, primarily as a result of the thrust exerted by the turbine on the flow. The velocity deficit will be greatest near the turbine and, due to turbulent mixing, diminish with distance downstream from the turbine such that the wake velocities eventually return to free-stream levels [1]. Unlike wind turbines, which only occupy a small fraction of the air column within which they sit, tidal turbines can occupy a large proportion of the limited water depth available in a channel. Indeed, in order to realize a significant fraction of a channel's potential to produce power, it is recommended that tidal turbines should occupy a large fraction of a channel's water depth [2]. The resulting blockage of flow due to the turbine's presence can lead to acceleration of the flow around the turbine (due to continuity). Structural drag will also lead to reductions in current velocities in the vicinity of the turbine due to frictional losses. Accurate calculations of the expected power output from a turbine must account for wake, blockage and drag effects.

Tidal turbine deployments to date have, almost exclusively, been single turbine devices; however, for economical reasons the natural progression of the industry is towards large multiple

device arrays. For example, the Meygen consortium proposes to deploy 3861 MW turbines in the Pentland Firth, Scotland [3]. Tidal flows are bi-directional and, due to the relationship between coastal topography and accelerated flow velocities, areas of high tidal stream resource availability also tend to be quite concentrated. The obvious approach to deployment of an array is, therefore, to place devices close together in a line perpendicular to the dominant direction of flow. However, physical constraints, such as channel width, available water depth and the presence of shipping lanes, will most likely necessitate the use of multiple rows of devices. This complicates the matter of estimating power yields, since the hydrodynamic effects of each turbine will influence the power available to neighbouring turbines and, by extension, the overall array output. Possibly of most importance is the spatial extents of the turbine wake as the placement of one turbine in the downstream wake of another will reduce the potential energy capture of the downstream device. Blockage effects will also be important as it may be possible to situate devices to make use of the accelerated flows caused by the blockages of other turbines (e.g., [4]).

Numerical modelling of tidal turbines involves two different scales. Near-field models are very highly resolved in three dimensions and employ mesh elements some orders of magnitude smaller than the diameter of the simulated turbine rotor. They are, therefore, ideally suited to the study of flow through and around a turbine (e.g., [5–14]); however, high computational costs have limited their application to the modelling of single (or very small numbers of) turbines in idealised channels, primarily under conditions of steady flow. Far-field models are typically two-dimensional (depth-averaged) and employ low spatial resolutions, typically orders of magnitude greater than the scale of the simulated turbine rotors. Their relatively low computational cost for large spatial extents make them ideally suited to modelling of large arrays in natural coastal systems. For example, reference [15] used a far-field model to investigate power output from a tidal turbine fence across a simple straight channel connecting two large basins, reference [16] assessed the hydro-environmental impacts of different configurations of a 2000 device array in the Severn estuary and reference [17] studied the impacts of various size arrays on tidal currents in the Tory Channel, New Zealand. The low spatial resolution of far-field models means that a single grid element typically contains multiple turbines. This method leads to errors in the power extracted by the turbine array as the variation in flow speed across the array is not modelled and the interactions between individual turbines are ignored [18].

In the present research, a 2D, nested, far-field model is modified to incorporate the mechanics of energy extraction by horizontal-axis tidal turbines and is then used to simulate an array of turbines at a spatial resolution equal to the diameter of the turbine rotors. The resolution of the nested domain is chosen so that each nested grid element is only large enough to enclose a single turbine. This allows the flows around individual turbines and interactions between adjacent turbines in an array to be resolved. This approach is similar to those of [19,20] who also use selective high resolution around turbines in 2D, depth-averaged, far-field models to capture the hydrodynamic interactions between adjacent turbines in arrays, with a view to optimising array layouts. Reference [19] used an irregular mesh to obtain the higher resolution while reference [20] used a regularly-spaced adaptive mesh. In the present model, the optimisation of array layouts is not conducted directly during the simulation; rather a number of simulations of single and twin turbine deployments are used to investigate turbine interactions with regard to power capture and the results are used to inform the optimum placement and spacing of turbines in a multi-row array. The model of [20] is also incapable of directly conducting optimisation of layouts and is used to compare the energy capture from arrays of different layouts. By comparison, reference [19] combined a gradient-based optimisation algorithm with a shallow water flow model to carry out optimisation in a single simulation whereby turbines are repositioned and flows recalculated in an iterative manner. The authors are currently working to develop such optimising functionality within our model.

This research is the first stage in a larger research project to develop the lowest-cost modelling solution (computationally speaking) for optimisation and management of tidal turbine arrays. A 2D

model with a basic turbulence scheme (the Prandtl mixing length model) was therefore employed in preference to a 3D model and/or a more complex, but more computationally expensive, turbulence scheme. While this approach has some obvious limitations, the results show that the general characteristics of the modelled turbine wakes (*i.e.*, spatial extents and velocity deficits) compare favourably to those recorded in published laboratory studies of scaled turbines. Section 2 of the paper describes how the mechanics of energy extraction were incorporated in the model by representing the turbine thrust as a sink term in the momentum equations. Section 3 describes the application of the model to an idealised tidal channel to simulate single and twin device deployments, and a 24-turbine multi-row array. Finally, results from the various model simulations are presented and discussed in Section 4 and conclusions provided in Section 5.

2. Methodology

The hydrodynamic model used for the research is the multi-scale nested model for (MSN_TT). This is an extension of the multi-scale nested model (MSN) developed at National University of Ireland Galway by Dr. Stephen Nash and Prof Michael Hartnett in 2009 [21–23]. MSN is a 2D, depth-averaged, finite difference, nested model which is based on the solution of the Navier-Stokes equations and takes account of the effects of local and advective accelerations, earth's rotation, barotropic and free surface pressure gradients, wind action, bed resistance and turbulence. MSN employs an overlapping grid structure with a single outer parent grid (PG) containing one or more nested child grids (CG). Each CG may also be a parent to further child grids so that one can achieve any desired spatial resolution. The model allows both one-way and two-way nesting. MSN has been extensively tested and validated for experimental and natural test cases (see [21–23] for details). (Note: MSN was in turn developed from the hydro-biological model DIVAST (depth integrated velocity and solute transport) [24] which has also been widely used and validated (e.g., [25,26])). MSN_TT was created by modifying MSN to simulate the impacts of tidal turbines and using one-way nesting to resolve the flow between neighbouring turbines.

2.1. Theory

MSN_TT computes water surface elevations and depth-integrated velocities by solving the depth-integrated continuity and momentum equations. The continuity and x-direction momentum equations are expressed by Equations (1) and (2) respectively as follows:

$$\frac{\partial \zeta}{\partial t} + \frac{\partial q_x}{\partial x} + \frac{\partial q_y}{\partial y} = 0 \tag{1}$$

$$\frac{\partial q_x}{\partial t} + \beta\left[\frac{\partial U q_x}{\partial x} + \frac{\partial V q_y}{\partial y}\right] = f q_y - gH\frac{\partial \zeta}{\partial x} + \frac{\tau_{xw}}{\rho} + \frac{\tau_{xb}}{\rho} + 2\frac{\partial}{\partial x}\left[\varepsilon H\frac{\partial U}{\partial x}\right] + \frac{\partial}{\partial y}\left[\varepsilon H\left[\frac{\partial U}{\partial y} + \frac{\partial V}{\partial x}\right]\right] \tag{2}$$

where ζ is water surface elevation (relative to mean water level), t is time, q_x and q_y are depth-integrated velocity flux components in the x- and y-direction, β is the momentum correction factor, U and V are depth-integrated velocity components in the x- and y-direction, f is the Coriolis parameter, g is gravitational acceleration, H is the total depth of the water column, τ_{xw} and τ_{xb} are the x-direction components of the surface wind stress and bed shear stress, respectively, ρ is fluid density and ε is the depth-averaged turbulent eddy viscosity. The turbulence model is a simple eddy viscosity model and was used specifically for its low computation cost in comparison with other higher order turbulence models.

A space-staggered orthogonal grid system is used with ζ specified at the centre of the grid cell, and q_x, U, H_x and q_y, V, H_y specified at the centres of the x- and y-direction cell faces, respectively. The finite difference scheme used in the model is based on the alternating direction implicit (ADI) technique where each timestep is sub-divided into two half-timesteps. Values of ζ, q_x and ϕ

are, therefore, computed for the first half-timestep and ζ, q_y and ϕ are computed for the second half-timestep.

For nesting, child grids may be telescoped to obtain any desired spatial resolution and the ratio of the PG spatial resolution to the CG spatial resolution, r_s, can be any whole integer value. CG solutions may also be refined in time as well as space and the ratio of PG to CG timesteps, r_t, can also be set to any integer value but is generally set to the same integer value as r_s. Figure 1 shows a schematic of the nested model domain.

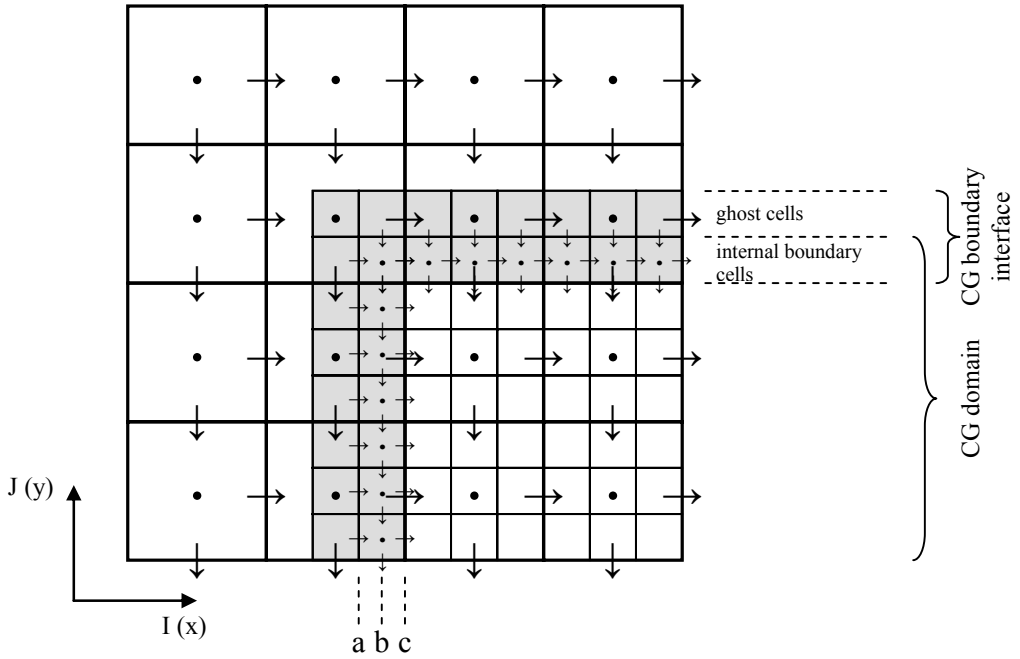

Figure 1. Schematic of the nested boundary configuration for a 3:1 spatial nesting ratio.

Conservation of mass and momentum at nested boundaries is extremely important for nested model accuracy. This is achieved in MSN_TT through an approach to the nested boundary formulation where ghost cells are introduced to the CG domain and used in the formulations of the CG open boundaries to essentially internalise them. The nested boundary ghost cell approach is demonstrated in Figure 1; for clarity CG variables are only shown for the boundary interface (shaded grey). Boundary data are interpolated from the PG and prescribed at the internal boundary cells and the ghost cells. At ghost cells, only velocity and flux components normal to the boundary require specification while all variable values are specified at internal boundary cells. See [22,23] for further details of the nesting procedure.

2.2. Numerical Approach to Representation of Turbines

A number of different approaches have been developed for modelling the dynamics of flow through, and around, tidal turbines. As would be expected the more complex of these are used in near-field models. In the sliding mesh model (SMM) approach (e.g., [7,8]) simulation of a rotating turbine is achieved by using a sliding mesh interface to enable a region of cells rotate within a larger, static grid. It is the most computationally expensive approach as it enables detailed simulation of the rotor motion and the resulting complex flows. The rotating (or moving) reference frame (RRF) approach (e.g., [8–11]) enables the simulation of rotating flows and uses detailed blade geometry to provide simulate the hydrodynamics around the turbine rotor including the downstream wake. The governing equations of flow are solved, in a reference frame which rotates at the same speed as the turbine, by the addition of Coriolis and centripetal forcing terms to the momentum equation. The blade element model (BEM) approach (e.g., [10–14]) models the time-averaged aerodynamic

effects of the rotating blades, without the need for creating and meshing the actual geometry of blades. The approach simulates the blade aerodynamic effects using a momentum source term placed inside a rotor disk fluid zone that depends on the chord length, angle of attack, and lift and drag coefficients for different sections along the turbine blade.

Actuator disc model (ADM) neglects blade geometry altogether and instead represents the turbine swept area as a porous disc. The influence of energy extraction is represented by inclusion of an extraction-related momentum sink in the momentum equation. This approach has been employed in both near-field (e.g., [6,27]) and far-field models [15]. Reference [28] have produced a refined ADM approach to inserting turbines in shock-capturing shallow water codes that is particularly useful. The most common approach in far-field models is to include the turbine thrust as a momentum sink in the momentum equations (e.g., [16,17,29]). The force is distributed evenly over the area of the grid cell. A final approach uses increased bed roughness to simulate the drag induced by energy extraction on the flow (e.g., [19,20,30,31]). Disadvantages of this approach are that it cannot account for the dimensions or performance characteristics of the turbine and energy is always captured from the flow regardless of the flow direction; this is unrealistic in the case of horizontal axis turbines whose orientation is typically fixed. Due to its relative simplicity and relative ease of implementation (implementation of the ADM approach for example would have required changing the solution scheme) and its ability to take account of turbine dimensions and orientation, the momentum sink approach was adopted in MSN_TT.

Figure 2 shows the flow through a horizontal-axis tidal turbine in a parallel-sided channel. The graphic identifies five stations: (1) far upstream of the turbine; (2) immediately upstream of the turbine; (3) immediately downstream of the turbine; (4) the region where the slower moving flow from the turbine's wake merges with the free stream fluid from the by-pass flow; and (5) adequately far enough downstream from the turbine that the pressure regains uniformity. The turbine takes momentum from the flow such that a reduction in velocity occurs across it; the result is the development of an area of reduced velocity downstream of the turbine - the wake. It can be seen that the undisturbed flow at (1) moves through the stream tube shown until it passes through the turbine (2–3) where it exerts a force on the turbine rotor. The turbine exerts an equal and opposite force, the thrust (T), on the flow which may be expressed as:

$$T = \frac{1}{2}\rho u^2 A_T C_T \tag{3}$$

where u is the upstream current velocity, A_T is the swept area of the turbine and C_T is the dimensionless thrust coefficient. C_T is a function of the turbine design and is dependent on the number of blades and their geometry.

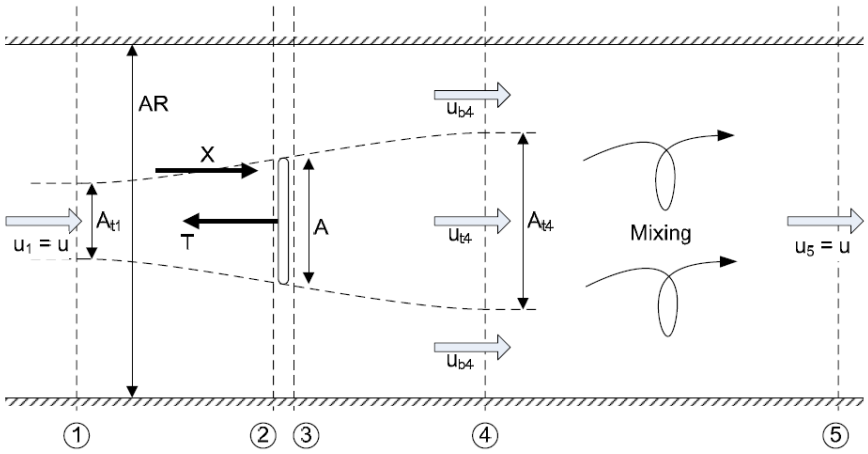

Figure 2. Linear momentum actuator disc model (ADM) in a parallel-sided channel (adapted from [28]).

The turbine thrust of Equation (3) is distributed evenly across the area of the enclosing grid cell to give a thrust-related stress which is then incorporated in the momentum equations. In other far-field studies where a grid element encloses multiple turbines, the total thrust from all enclosed turbines is calculated and distributed across the plan area of the grid element. Assuming that the angle which the turbine axis makes with the positive y-axis is θ, then, the x- and y-components of the stress induced by the turbine thrust, $\boldsymbol{\tau}_{Tx}$ and $\boldsymbol{\tau}_{Ty}$, may be calculated as:

$$\tau_{Tx} = (T/\Delta x \Delta y) \,.\, |\sin\theta| \,.\, (|U|/U) \tag{4}$$

$$\tau_{Ty} = (T/\Delta x \Delta y) \,.\, |\cos\theta| \,.\, (|V|/V) \tag{5}$$

where U, V and Δx, Δy are the current velocity components and the grid spacings, respectively, in the x- and y-directions. $(|U|/U)$ and $(|V|/V)$ account for flooding and ebbing tides so that the thrust always acts to slow the flow. Equations (4) and (5) take account of the angle of orientation of the turbine to the flow; this means that the model is suitable for both rectilinear and non-rectilinear flows. In the present approach, the spatial resolution was set equal to the rotor diameter such that a grid element only contained a single turbine; the use of lower resolutions is not recommended as the model will be unable to capture the flow between adjacent turbines. Higher spatial resolutions can be used but in such instances the swept area of the turbine A_T will be distributed across a number of grid cells and T is therefore calculated for each grid cell based on the proportion of A_T lying within the grid cell.

The thrust induced by the turbine on the flow does not incorporate the drag induced by the support tower of the turbine. This structural drag force, D, is calculated in a manner similar to that used to compute the drag induced by bottom roughness as follows:

$$D = \frac{1}{2}\rho u^2 A_S C_D \tag{6}$$

where A_S is the projected area of the turbine tower support and C_D is the dimensionless drag coefficient. Similar to the turbine thrust, the drag is incorporated in the momentum equations as a drag-related stress, where the x- and y-components of the stress are calculated as:

$$\tau_{Dx} = (D/\Delta x \Delta y) \,.\, |\sin\theta| \,.\, (|U|/U) \tag{7}$$

$$\tau_{Dy} = (D/\Delta x \Delta y) \,.\, |\cos\theta| \,.\, (|V|/V) \tag{8}$$

The x-direction momentum equation (and similarly for the y-direction) was amended as follows to include the x-components of the turbine thrust and structural drag:

$$\frac{\partial q_x}{\partial t} + \beta\left[\frac{\partial U q_x}{\partial x} + \frac{\partial V q_y}{\partial y}\right] = f q_y - gH\frac{\partial \zeta}{\partial x} + \frac{\tau_{xw}}{\rho} - \frac{\tau_{xb}}{\rho} + 2\frac{\partial}{\partial x}\left[\varepsilon H \frac{\partial U}{\partial x}\right] + \frac{\partial}{\partial y}\left[\varepsilon H\left[\frac{\partial U}{\partial y} + \frac{\partial V}{\partial x}\right]\right] - \frac{\tau_{Tx}}{\rho} - \frac{\tau_{Dx}}{\rho} \tag{9}$$

In addition to generation of thrust and drag forces, tidal turbines also generate turbulence. However, due to the use of a simplistic turbulence model and the fact that parameterisation of turbulence models can be computationally expensive [32], turbulence generation by the turbines is not included in the present model.

The power, P, captured by a tidal turbine can be calculated as:

$$P = \frac{1}{2}\rho u^3 A_T C_P \tag{10}$$

where C_P is the dimensionless power describing the efficiency of the turbine. Data for both horizontal-axis [1,33] and vertical-axis turbines [34] show there is a relationship between C_P and C_T. Although the relationship is non-linear, these data confirm that the thrust coefficient is greater than the power coefficient. For unblocked flows, it can be shown that the theoretical maximum C_P is 0.59 and that this is achieved for C_T = 0.9 [28]. However, it has been shown that this limit can be exceeded

for tidal turbines where the turbines occupy a large proportion of the channel cross-section (e.g., [35]). Mechanical losses will act to reduce the theoretical C_P. Experimental tests of scaled horizontal-axis turbines by [1] recorded a maximum C_P of 0.46 and a corresponding C_T of 0.8 (for a blade pitch angle of 20°) while the high resolution near-field modelling study of [33] recorded a maximum C_P of 0.4 and a corresponding C_T of 0.88 (for a blade pitch angle of 6°). These values of C_P and C_T were recorded for particular flow speeds and C_P and C_T will vary with flow speed across the turbine. In addition, a turbine will typically have a cut-in flow speed below which no power is generated and thus both C_P and C_T are zero, and a rated flow speed above which the power output is limited such that C_P and C_T both decrease with increasing flow speed. For simplicity, and to allow comparison with the porous disc experiments of [5], the present research employs a constant C_T of 0.8.

3. Numerical Simulation

The model was applied to an idealised rectangular channel (Figure 3), 5000 m long and 600 m wide, which was subject to tidal flows. The channel had a flat bed with 20 m mean water depth. The bed roughness height was specified as 50 mm. A repeating tide of 4 m amplitude and 6.25 h period was specified at the western sea boundary; the remaining three boundaries were closed land boundaries defined using a no-slip condition. The short tidal period was employed to affect tidal velocities in the range of those employed in the experimental studies of [5], *i.e.*, approximately 0.2 m/s. (These velocity magnitudes are outside of the operating range of most tidal turbines and given that the model results are particular to the simulated domain and flow conditions, care should be taken when applying the findings to other domains and flow conditions.)

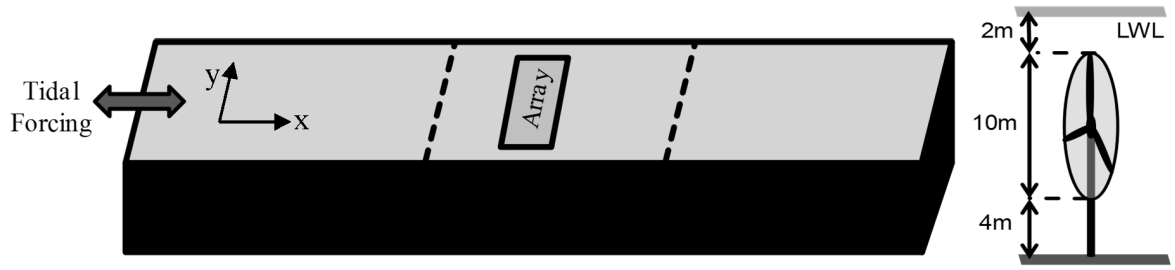

Figure 3. The modelled idealised channel showing the approximate location of the turbine array and the tidal turbine arrangement. Dashed lines indicate extents of the nested domain.

The simulated turbines comprised a single rotor, 10 m in diameter, mounted on a 1 m diameter cylindrical support tower (Figure 3). The child grid horizontal spatial resolution was set at 10 m to match the turbine rotor diameter so that flow between turbines could be simulated. A 5:1 spatial nesting ratio was employed meaning the PG resolution was 50 m. Figure 3 shows the upstream and downstream extents of the nested domain. The turbine array was placed at the centre of the channel within the nested domain. Figure 4 compares a section of the coarse grid and nested meshes to demonstrate the improved resolution between adjacent turbines while the model setup is summarised in Table 1. For the vertical position of the turbine in the water column, a 2 m clearance was assumed between the upper limit of the rotor swept area and the low water level (Figure 3). This resulted in a 9 m high support tower. Even though 5 m of the support tower would be shielded by the turning rotor, the full height of the tower was used to calculate A_S in Equation (6) giving A_S = 9 m^2. A drag coefficient of 0.9 was used for all turbine simulations.

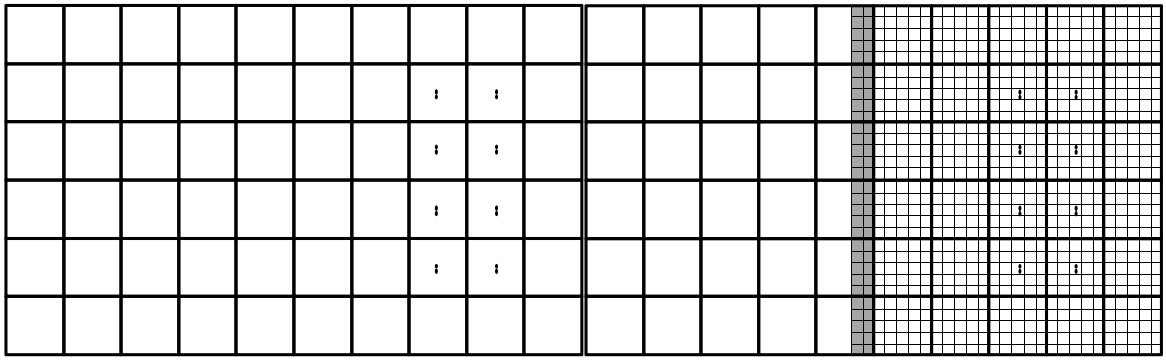

Figure 4. Example of positioning of 10 m rotor diameter turbines on a 50 m coarse resolution grid (left) and a 10 m nested high resolution grid (right) using 5 rotor diameters (RD) spacings in both the lateral and longitudinal directions. Shaded cells are the boundary interface of the nested domain.

To extract the maximum energy from a flow, the turbine swept area should be oriented perpendicular to the primary direction of flow. For the majority of horizontal axis turbines this orientation is fixed, *i.e.*, the turbine rotor cannot swivel about the support tower axis, and so the same restriction was applied to the simulated turbines. Since the primary direction of flow was in the x-direction (Figure 3), the y-component of the turbine thrust (Equation (5)) was set to zero. Structural drag was applied in both component directions. During development, the model performance was assessed by comparison of modelled wake velocity deficits with published data from [5]. The structural drag coefficient was used as the calibration parameter and best agreement between modelled and measured data was achieved for C_D = 0.9. This is in line with the drag coefficient for a smooth cylinder which ranges from 0.4 to 1.2 for Reynolds Numbers from 1×10^4 to 1×10^7 [34].

Table 1. Summary of idealised channel model setup.

Physical Parameter	Domain	
	Parent Grid: PG	Child Grid: CG
L_X	5.0 km	1.5 km
L_Y	0.6 km	0.6 km
Water depth	20 m	20 m
Tidal amplitude	4 m	4 m
Tidal period	6.25 h	6.25 h
Grid SPACING	50 m	10 m
Timestep	12 s	60 s
No. of grid cells	2400	9000
Bed roughness	50 mm	50 mm

4. Numerical Simulation Results

To assess the model's ability to capture general wake characteristics, a single turbine deployment was first considered in the centre of the study area. To investigate the interaction between adjacent turbines, a number of simulations were next conducted of two turbines deployed at different lateral spacings. The results of these initial studies helped to determine optimal lateral and longitudinal spacings which were, in turn, used to devise an optimised layout for a 24 turbine multi-row array. Finally, to determine the effect of the optimised array layout on power yield, the energy capture of a comparable regularly-spaced array was compared with that of the optimised array. All model simulations were run for four tidal cycles. In all instances, cold start effects had dissipated by the end of the first tidal cycle. All model results are presented for the final tidal cycle.

As already stated the nested 2D model with low-cost turbulence scheme was selected for assessment as a low-cost solution. The model has some obvious limitations with regard to the modelling of turbine wakes which must be considered when analysing results. First, as it is depth-averaged in the vertical plane the model cannot capture the full 3D wake structure and the velocity deficits computed in the turbine wake are averaged over the water column. Second, the basic turbulence model means it cannot fully reproduce the complex dynamics of wake mixing. While these limitations are important to bear in mind, the model was assessed based on its ability to capture the general characteristics (spatial extents and velocity deficits) of the turbine wakes, rather than their exact detail, with a view to identifying the optimum positioning of turbines in an array.

4.1. Single Turbine

Figure 5a shows the current vectors at mid-flood (23.0 h) when the single turbine was included in the model. The black square indicates the location of the turbine and grid units are measured in rotor diameters (RD) from the turbine. Figure 5b shows the percentage difference in mid-flood current speeds when the turbine is included to those computed without any turbines (*i.e.*, %DIFF = $100(U_{\text{turb}} - U_{\text{no turb}})/U_{\text{no turb}}$). As would be expected, the turbine has a readily noticeable effect on the flow; in particular, the wake (*i.e.*, the area of reduced velocities downstream of the turbine) is clear visible. A similar wake is observed on the opposite side of the turbine on ebb tides. Areas of accelerated flows can be observed to either side of the wake; these are accelerated bypass flows caused by the blockage effect of the turbine.

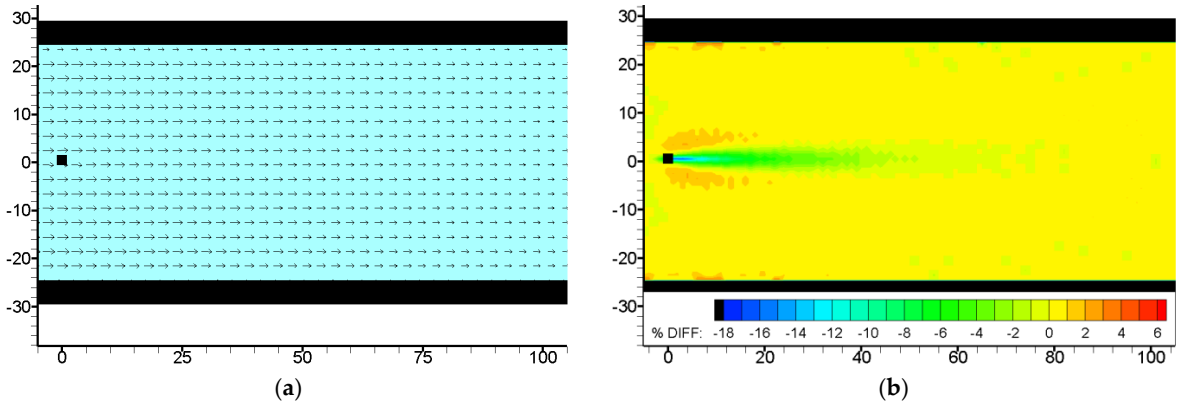

Figure 5. (**a**) Current velocity vectors and (**b**) percentage change in current speeds at mid-flood for a single turbine (Note: in (**a**) vectors are only shown at every fourth grid cell).

Figure 6a shows the % changes in current speed (negative = reductions) extracted from Figure 5b along the longitudinal wake centreline. The largest reduction in current speed, approximately 16%, was recorded immediately downstream of the turbine. As the wake recovers, velocity reductions decrease with distance downstream of the turbine. By 40 RD downstream the reductions in speed have dropped to approximately 2% and by 70 RD freestream flow conditions have been resumed. The % changes in current speed of Figure 6a were converted to longitudinal velocity deficits ($1 - U_{\text{turb}}/U_{\text{no turb}}$) to allow comparison with the measurements of [5] who studied the impacts of a single rotor turbine on flow in a recirculating flume using porous discs as turbine proxies. Reference [5] measured longitudinal velocity deficits along the turbine centreline as well as velocity deficits through the water column at selected downstream distances. The vertical deficit profiles were bell-shaped, with the deficit being highest at the centre of the turbine and decreasing to almost zero at the top and bottom of the turbine swept area.

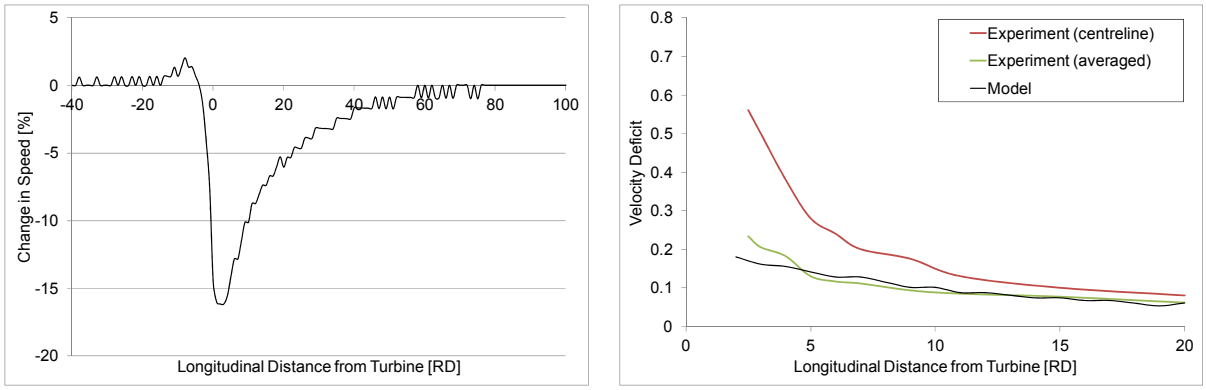

(**a**) (**b**)

Figure 6. (**a**) Changes in current speed along the longitudinal wake centreline and (**b**) comparison of modelled and measured velocity deficits along the same centreline.

Given that the current model is depth-averaged, it is unable to compute the variation in velocity deficit through the water column and instead computes the depth averaged deficit. Thus, to facilitate comparison of modelled and measured deficits, depth-averaged values of the measured longitudinal velocity deficits [5] were calculated at all of the downstream distances at which full water column measurements were available. Figure 6b compares the depth-average modelled and measured longitudinal deficits. The deficits measured at the turbine centreline are also included for reference; as would be expected there is a significant difference between the measured centreline and depth-averaged values. For the depth-averaged deficits however, there is very good agreement between the modelled and measured values beyond a downstream distance of 4 RD. Figure 6b confirms that the rate of velocity recovery and the longitudinal extent of the wake computed by the model compare very favourably to those observed in the experiment. At downstream distances less than 4 RD the modelled velocity deficits are lower than the measured data. This may be due to the relative coarseness of the model resolution relative to the turbine diameter and the inability of the 2D model to simulate the complex 3D flow through and around the turbine. To resolve this issue, a two-way nested, 3D version of the present model is currently in development that will provide both higher resolution and three-dimensional flows.

Figure 7 plots the changes in current speed (again expressed as velocity deficits) along 5 lateral transects (2 RD, 4 RD, 10 RD, 20 RD and 40 RD downstream) through the modelled turbine wake. It can be seen that the wake is symmetrical about the centre of the turbine, exhibiting a bell-shaped profile, and that its width increases with distance downstream, growing from 2 RD width at 2 RD downstream to 6 RD width at 20 RD downstream. This is in agreement with the findings of [36] who studied the wake of a single scale model rotor in a recirculating flume; their wake exhibited a symmetrical, approximately bell-shaped, lateral profile, an increase in wake width with distance downstream and a comparable wake width of 2 RD at 4 RD downstream. If one assumes a similar vertical profile for the wake recorded by [36] to that recorded by [5],at the common measurement location of 4 RD downstream then one can compute a depth-averaged value for the centreline deficit of [36] of 0.18; the corresponding modelled value at 4 RD is 0.16 (from Figure 7). These comparisons serve to demonstrate that the lateral extents of the modelled wake compare favourably with experimental measurements.

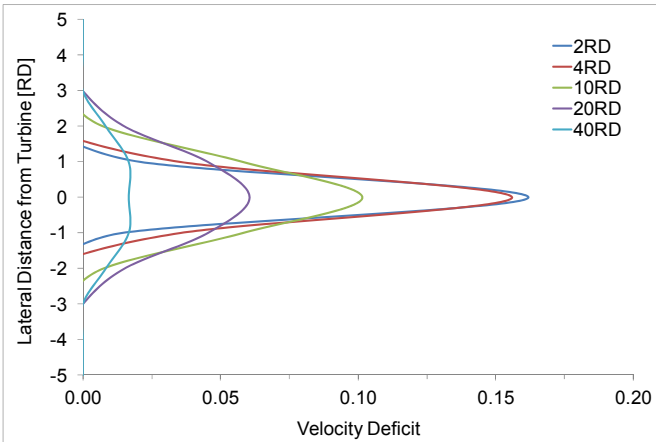

Figure 7. Velocity deficits along a number of lateral transects through the modelled turbine wake.

Looking at the turbine itself, Figure 8a compares the variation in current speeds over a single tidal cycle at the location of the turbine with and without the turbine in place. Similar levels of reductions in current speed are observed on both the ebb and flood tides. Figure 8b shows the power extracted by the turbine over a tidal cycle. By integrating this power curve over the tidal cycle the total energy extracted by the turbine was calculated at 204 Wh per tidal cycle.

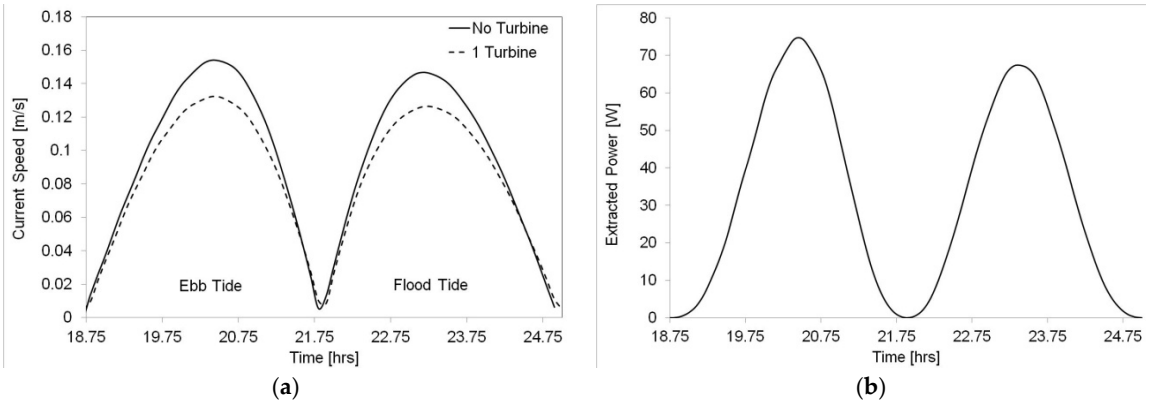

(**a**) (**b**)

Figure 8. (**a**) Time series of current speeds at the location of the turbine with and without the single turbine and (**b**) time series of power capture by the turbine over a tidal cycle.

Reference [37] have shown that, depending upon wave period and direction, the prevailing wave climate at a site can affect the available tidal stream resource by as much as 10% and they suggest that coupled wave-tidal models may be required for accurate resource assessment and turbine impact studies. With regard to the low-cost modelling solution used here, the inclusion of a wave module would have significantly increased the computational time. However, [36] also studied the effects of waves on turbine wake characteristics and found that for the case of irregular waves opposing the direction of current flow there was no change in the vertical and lateral wake profiles and while there was a decrease in the velocity deficit immediately downstream of the turbine, beyond 10 RD downstream, the velocity deficits were similar to those generated in the absence of waves. Given that the author's model is primarily concerned with far-field wake characteristics, the findings of [36] suggest that the inclusion of a wave module is unnecessary.

4.2. Two Turbines

When turbines are deployed in close proximity, it is possible for the turbines to interact such that the effects of one turbine on the prevailing flow will affect the energy capture by another.

In order to investigate these interactions and determine optimal spacings between turbines, a number of simulations were conducted of two turbines deployed at different lateral spacings (Figure 9a). 11 spacings were investigated ranging from 0 to 10 RD. Figure 9b plots the total energy capture per tidal cycle for the turbines in the 2 RD simulation; in all simulations each turbine captured half of the total energy yield.

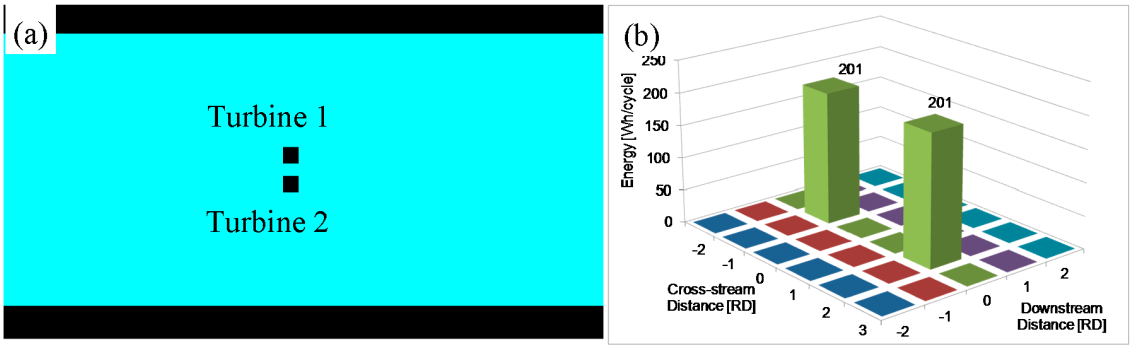

Figure 9. (**a**) Turbines in 2 RD simulation and (**b**) energy captured by each turbine.

Figure 10 compares the changes in current speeds caused by turbines deployed at 1 RD lateral spacing with those at 10 RD spacing. For the 1 RD lateral spacing, the wakes from each turbine merge into a single wake a short distance downstream of the devices whereas two distinct wakes are formed for the 10 RD spacing, each of which show the same characteristics as that of the single isolated turbine. Figure 11 compares lateral velocity deficits through the turbine wakes at distances 2 RD, 4 RD and 10 RD downstream of the turbines for lateral spacings of 1 RD, 2 RD, 3 RD and 4 RD. Since the turbines were placed equidistant from the channel centreline (see Figure 10b), *i.e.*, lateral distance of 0 RD, velocity deficits at 0 RD greater than zero thus indicate that the wakes have merged while deficits equal to or less than zero mean merging has not occurred. For the 1 RD spacing, immediate wake merging is evident with a velocity deficit present at 0 RD, *i.e.*, the centreline between the two turbines. The magnitude of this deficit increases such that at 10 RD it is greater than the deficits at the turbine centrelines. The fully merged wake at 10 RD is symmetrical and exhibits an approximate bell-shaped distribution similar to that of a singular turbine wake. The lateral deficit profiles show that wake merging does not occur when a lateral spacing of 3 RD or greater is employed; at these spacings the lateral deficits are very similar to those for a single isolated turbine. These observations agree with the findings of [36] who also studied the interactions between turbine wakes for different layouts of a group of scaled three-bladed rotors and noted that for lateral spacings less than 2 RD the wakes of adjacent turbines merged but for spacings of 3 RD and greater the wake of each rotor was very similar to that of an isolated rotor.

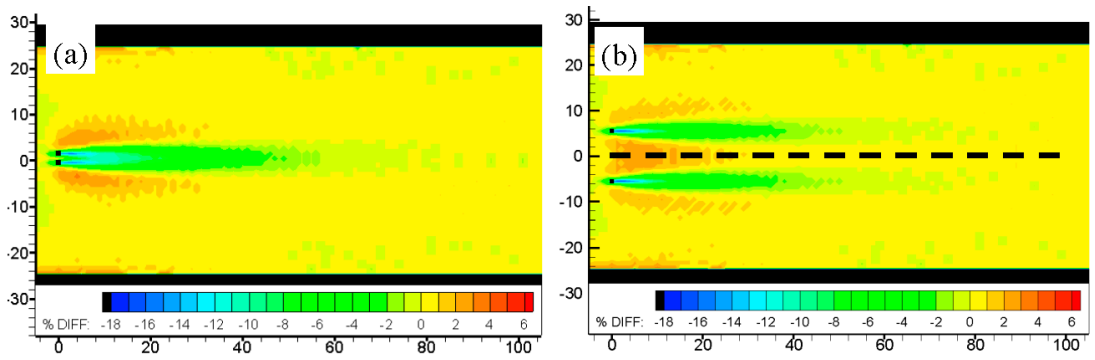

Figure 10. Changes in current speeds for two turbines deployed at (**a**) 1 RD and (**b**) 10 RD lateral spacing.

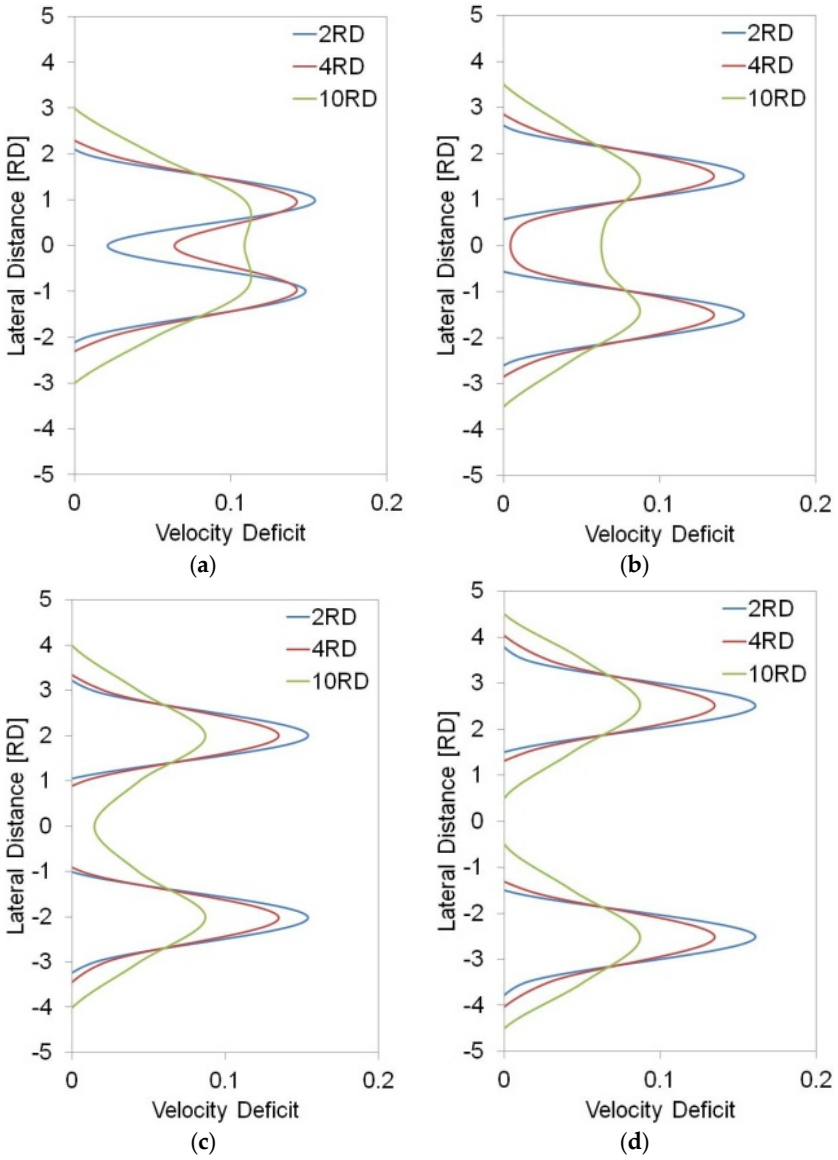

Figure 11. Lateral velocity deficits downstream of two turbines deployed at: (**a**) 1 RD; (**b**) 2 RD; (**c**) 3 RD and (**d**) 4 RD lateral spacings.

The turbine wakes in Figure 10b show acceleration of flows outside, and between, the two turbines. This is also consistent with scale model studies. For example, [38] studied the wakes of small arrays of turbines, using scale model mesh discs as proxies, and noted that flow acceleration between devices, induced by blockage effects, increased with reducing lateral spacing; a 22% increase in kinetic energy was achieved for an optimal lateral spacing of 1.5 RD. The accelerated flows outside the turbines are due to blockage effect of the turbines and can also be seen for the single turbine (Figure 3b). The accelerations between the turbines are due to both blockage effects and to the closely-spaced turbines, and their wakes, inducing a venturi effect on the flow. Given that available power is a function of velocity cubed, these areas of intra-turbine accelerated flows could be considered as optimal locations when considering the placement of turbines in an array. The maximum acceleration between turbines occurs along the dashed centreline axis of Figure 10b. The lateral spacing which induces the greatest accelerations was identified by comparing the changes in current speed along this centreline (see Figure 12).

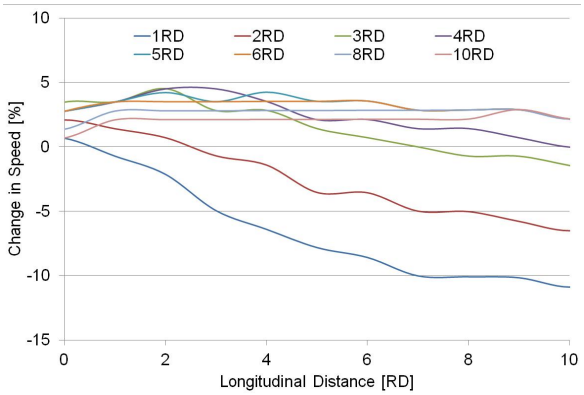

Figure 12. Change (%) in current speed along the longitudinal axis of Figure 8b.

Looking firstly at the change in speed for the 1 RD spacing, a small increase in speed occurs at 0 RD downstream but beyond this reductions in speed promptly occur. This is explained by our earlier finding that the use of a 1 RD lateral spacing results in almost immediate merging of wakes. This merging of the wakes means the speed continues decreasing to a downstream distance of approximately 10 RD after which the velocity begins to recover. A similar pattern is observed for the 2 RD lateral spacing but with merging occurring slightly further downstream at 2 RD. The largest increases in speed of 4.5%, was recorded for the lateral spacings of 3 RD and 4 RD. Similar, but slightly lower increases were observed for 5 RD and 6 RD spacings. Peak increases in speed were lowest for the 2 RD and 1 RD spacings, most likely due to the spacing being too small and consequently acting to restrict the flow between the turbines. Peak increases were also smaller for spacings of 8 RD and greater due to the turbines and their wakes being too far apart to induce a venturi effect. The results suggest that in order to induce accelerations in flow and, therefore, increase the power available to a suitably placed downstream turbine in an array, an optimal lateral spacing of between 3 RD and 4 RD should be employed. Figure 9 also suggests that the optimal longitudinal spacing for the placement of the downstream turbine to intercept the accelerated flows lies between 1 RD and 4 RD, as beyond this the increases in speed begin to drop.

4.3. Array

The initial turbine simulations indicated that a multi-row array in which turbines were placed in-line would suffer from reduced efficiency due to adverse interactions between turbines, namely, the wakes of some turbines reducing the power availability to others. The conclusions as to the optimal array layout suggested one should use:

(1) A staggered array formation in which downstream turbines do not significantly interact with the wakes of upstream turbines thus allowing the use of a relatively small longitudinal spacing.
(2) A lateral spacing that would induce flow acceleration which downstream turbines could then intercept—the results suggested an optimal spacing of between 3 RD and 4 RD.
(3) A longitudinal spacing that would place downstream turbines within the region of highest flow acceleration—the results suggested an optimal spacing of between 1 RD and 4 RD.

It was proposed to use four rows of six turbines for a staggered multi-row array. To induce flow acceleration between turbines a 4 RD lateral spacing was selected. The longitudinal spacing had to be large enough to allow adequate flow through the array so that intra-turbine accelerations could develop between downstream turbines; 4 RD was therefore also selected as the longitudinal spacing. The same spacings were used for the in-line, regularly-spaced array so that both arrays had similar spatial extents allowing comparisons between the two. The array layouts are shown in Figure 13. Figure 14 shows changes in mid-flood current speeds due to inclusion of the tidal arrays and the energy capture by individual turbines over the course of a tidal cycle.

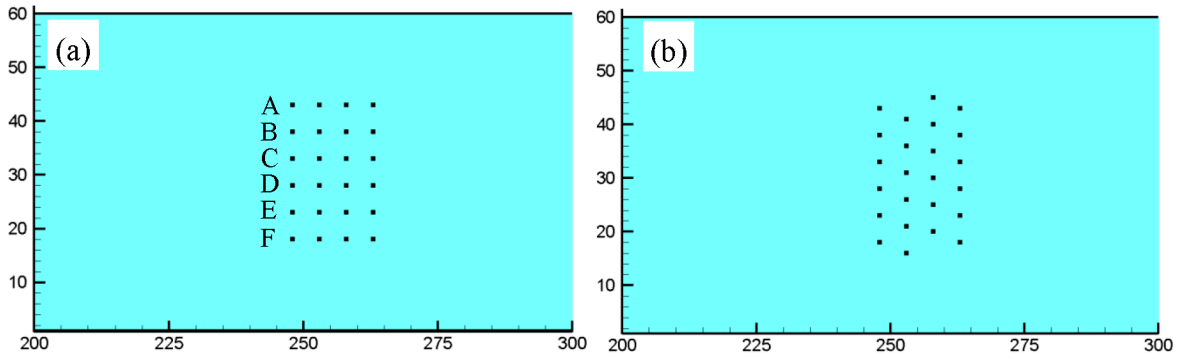

Figure 13. Layouts of (**a**) the in-line, regularly-spaced array and (**b**) the staggered array.

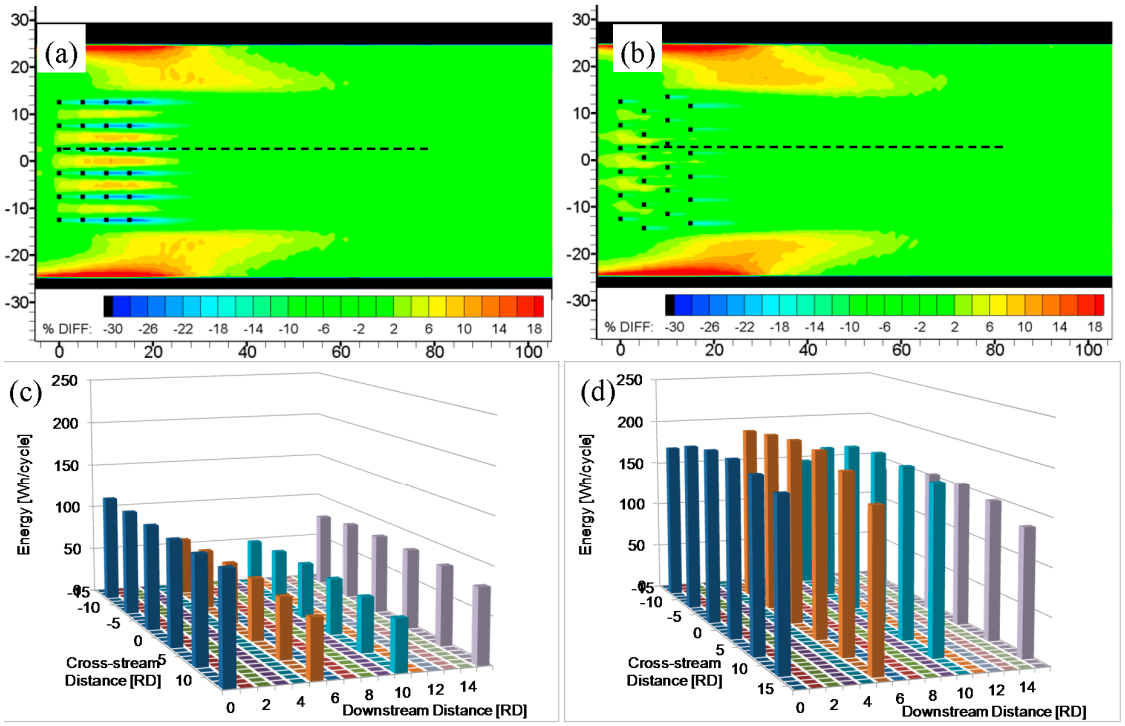

Figure 14. (**a**,**b**) Changes in current speed and (**c**,**d**) energy capture for the in-line and staggered arrays, respectively.

The energy captured by the turbines in the in-line array is clearly much lower than that captured by the turbines in the staggered array. Summing the energy capture of each turbine, the total energy capture of the in-line array was 1917 Wh per tidal cycle, compared with 4124 Wh per tidal cycle for the staggered array. The poor performance of the in-line array is due to the positioning of downstream turbines in the wakes of upstream turbines, while the performance of the staggered array is boosted by making use of the accelerated flows between turbines.

Looking at the in-line array, the energy capture of the turbines in Row 4 of the array (*i.e.*, at 15 RD downstream distance) was roughly half that captured by the single turbine of Section 4.1. This is because the power extraction and combined wake effects of the upstream turbines in Rows 1, 2 and 3 result in reduced flow speeds, and thus available power, to the turbines in Row 4. These effects are easily seen in Figure 15 which plots the mid-flood velocity deficits along the longitudinal transect shown in Figure 14a. Corresponding deficit plots for the staggered array and the single turbine of Section 4.1 are included for comparison. For the in-line array, the cumulative effect of energy extraction by each subsequent downstream turbine means the velocity deficit increases through the

array, reaching a maximum at the fourth row turbine (at 15 RD downstream), and the magnitude of the maximum deficit is much greater than that for the single turbine, 0.27 *versus* 0.16. On ebbing tides, the first row of turbines (at 0 RD downstream) experience similar reductions in available power to the fourth row turbines. The inner turbines in Rows 2 and 3 experience reduced flow speeds on both ebb and flood tides and their energy capture is, therefore, significantly lower than the outer turbines.

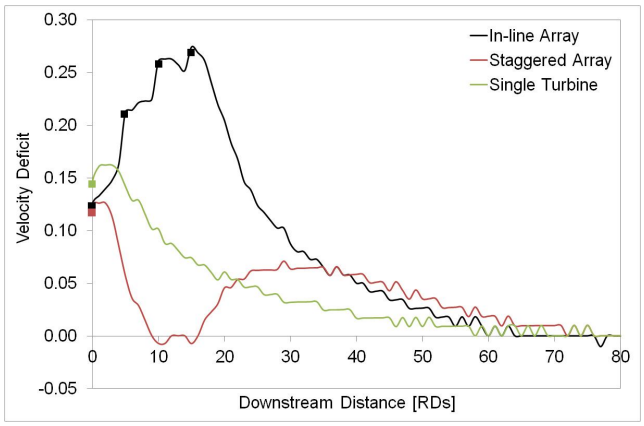

Figure 15. Longitudinal velocity deficits for the in-line and staggered arrays plotted along the transects in Figure 11a,b and along the centreline through a single isolated turbine (the squares indicate turbine locations).

Staggering the turbines so that downstream turbines are placed outside the wakes of adjacent turbines and so that they intercept the accelerated flows induced by upstream turbines significantly improves the energy capture of the array. By comparison with the regularly-spaced array, the energy capture of the inner turbines in the staggered array is actually higher than that of the outer turbines. This is due to the inner turbines intercepting accelerated flows induced by adjacent turbines on both stages of the tide whilst the outer turbines only experience such accelerated flows on one stage of the tide. Although some turbines from different rows (the first and third for example) are almost in-line, they are sufficiently far apart (15 RD) that velocity recovery can take place in the wake of the upstream turbine before the flow reaches the downstream turbine. Figure 15 demonstrates the point. The longitudinal deficit profile shown for the staggered array passes through a first row turbine at 0 RD downstream which is almost in line with a third row turbine at 10 RD downstream. The third row turbine should therefore lie within the wake of the first row turbine; however, it can be seen from Figure 15 that by 10 RD downstream, the velocity deficit in the wake of the first row turbine has decreased to zero and thus the power availability to the 3rd row turbine is unaffected. The rate of recovery of the first row turbine wake in the staggered array is much faster than that for the single turbine; this is due to increased shear mixing of the wake with the accelerated flows caused by the turbines to either side (see Figure 11a).

The aim of this research is to develop a low-cost solution modelling system for optimizing array layouts. The computational saving is achieved by using nesting to obtain high resolution around the turbines. The saving was measured by comparing the model runtime against a model system that employed the same approach for representing the turbines but employed a high spatial resolution across the full model domain. A 62% saving in computational runtime was achieved for the idealized channel domain presented here; however, the saving is obviously dependent on the extents of the nested domain.

5. Conclusions

A far-field numerical model, MSN_TT, was developed to simulate the turbine effects and energy yields of tidal turbines. The mechanics of energy extraction were included in the model

by representing the turbine thrust as a drag force in the momentum equations. The effect of structural drag was also included in the model. The model was first assessed for its ability to simulate the general wake characteristics of individual turbines. A 2D model with a basic eddy-viscosity turbulence model was specifically chosen for its low computational cost and, even with these limitations, the model was found to give good agreement with published experimental data. Consequently the model was used to investigate interactions between turbines with a view to identifying optimum spacings and layouts for multiple device arrays.

The following conclusions can be drawn from the research:

- Far-field models allow simulation of large multiple device arrays, and using nesting to obtain a spatial resolution equal to the simulated turbine rotor diameter allows such models to capture the wake and blockage effects of individual turbines and the resulting interactions between turbines, all of which have a significant impact on the potential energy capture of an array.
- Not-withstanding the model limitations, the modelling approach enables computation of turbine wakes of similar spatial extents and velocity deficits to those recorded in published scaled-turbine experiments. The interactions between devices computed by the model, such as wake merging and intra-turbine accelerations, also compare favourably with the same processes noted in published experimental studies.
- For a single isolated turbine, deceleration of flow occurs in the turbine wake. Wake recovery, due to downstream mixing, subsequently results in the dissipation of power losses with distance downstream and a return to ambient flow conditions. Model results indicate that this occurs at a distance of approximately 70 RD; two in-line turbines placed within 70 RD of each other will therefore experience reduced power availability on either ebbing or flooding tides. Velocities were found to return to within 2% of undisturbed levels at 40 RD; this could be considered an acceptable longitudinal spacing for in-line turbines but is not practical given the limited spatial extents of high energy tidal stream sites.
- The lateral spacing between turbines can be tuned to induce flow acceleration, which can, in turn, be harnessed by appropriately placed downstream turbines. The research indicates that an optimal lateral spacing for inducing acceleration between turbines is 3 RD and 4 RD and an optimal longitudinal spacing for downstream turbines to intercept accelerated flows is 1–4 RD. The use of larger longitudinal spacings will position the downstream turbine outside of the area of peak accelerations.
- A staggered array layout is recommended, where downstream turbines are placed such that they intercept the accelerated flows induced by upstream turbines and avoid the wakes of adjacent turbines. A staggered array using 4 RD lateral and longitudinal spacings resulted in an energy yield per tidal cycle of more than twice that of a comparable in-line array.

The conclusions regarding optimal spacings relate to the conditions and turbine (horizontal axis single rotor) that were simulated in the research and these spacings may not be optimal for all flow conditions and/or turbines. The generation of turbulence by the turbines is not included in the present model. Research has shown that turbulence generation can affect wake characteristics and thus available power. In particular, it has been shown that wake recovery is faster behind turbines generating greater turbulence [20,39]. The wake lengths of the present model should be interpreted in this context and the model will be further developed to investigate the effects of turbulence generation on wake properties and energy capture.

Acknowledgments: This research was carried out with the support of funding from the following sources:

- Marine Renewable Energy Ireland (MaREI) which is supported by Science Foundation Ireland under Grant No. 12/RC/2302.
- The MAREN2 project which is part-funded by the European Regional Development Fund (ERDF) through the Atlantic Area Transnational Programme (INTERREG IV).

- The ENERGYMARE project which is part-funded by the European Regional Development Fund (ERDF) through the Atlantic Area Transnational Programme (INTERREG IV).

Author Contributions: Stephen Nash did the numerical modelling and wrote the paper. Agnieszka Olbert and Michael Hartnett reviewed and edited the manuscript. All authors read and approved the manuscript.

Conflicts of Interest: The authors declare no conflict of interest.

References

1. Bahaj, A.S.; Molland, A.F.; Chaplin, J.R.; Batten, W.M.J. Power and thrust measurements of marine current turbines under various hydrodynamic flow conditions in a cavitation tunnel and a towing tank. *Renew. Energy* **2007**, *32*, 407–426. [CrossRef]
2. Vennell, R. Tuning turbines in a tidal channel. *J. Fluid Mech.* **2010**, *663*, 253–267. [CrossRef]
3. Meygen. The Meygen Project. Available online: http://www.meygen.com/ (accessed on 17 June 2013).
4. Divett, T.; Vennell, R.; Stevens, C. Optimization of multiple turbine arrays in a channel with tidally reversing flow by numerical modelling with adaptive mesh. In Proceedings of the 10th European Wave and Tidal Energy Conference, Southampton, UK, 5–9 September 2011.
5. Bahaj, A.S.; Myers, L.E.; Thomson, M.D.; Jorge, N. Characterising the wake of horizontal axis marine current turbines. In Proceedings of the 7th European Wave and Tidal Energy Conference, Porto, Portugal, 11–14 September 2007.
6. Sun, X.; Chick, J.P.; Bryden, I.G. Laboratory-scale simulation of energy extraction from tidal currents. *Renew. Energy* **2008**, *33*, 1267–1274. [CrossRef]
7. McNaughton, J.; Afgan, I.; Apsley, D.D.; Rolfo, S.; Stallard, T.; Stansby, P.K. A simple sliding-mesh interface procedure and its application to the CFD simulation of a tidal-stream turbine. *Int. J. Numer. Methods Fluids* **2014**, *74*, 250–269. [CrossRef]
8. Lawson, M.; Li, Y.; Sale, D. Development and verification of a computational fluid dynamics model of a horizontal-axis tidal current turbine. In Proceedings of the 30th International Conference on Ocean, Offshore, and Arctic Engineering, Rotterdam, The Netherlands, 19–24 June 2011.
9. O'Doherty, D.M.; Mason-Jones, A.; O'Doherty, T.; Byrne, C.B. Considerations of improved tidal stream turbine performance using double rows of contra-rotating blades. In Proceedings of the 8th European Wave and Tidal Energy Conference, Uppsala, Sweden, 7–10 September 2009.
10. Javaherchi, T.; Stelzenmuller, N.; Seydel, J.; Aliseda, A. Experimental and Numerical Analysis of a Scale-Model Horizontal Axis Hydrokinetic Turbine. In Proceedings of the 2nd Marine Energy Technology Symposium, Seattle, WA, USA, 15–17 April 2014.
11. Mozafari, J.; Teymour, T. Numerical Investigation of Marine Hydrokinetic Turbines: Methodology Development for Single Turbine and Small Array Simulation, and Application to Flume and Full-Scale Reference Models. Ph.D. Thesis, University of Washington, Seattle, WA, USA, 2014.
12. Willis, M.; Masters, I.; Thomas, S.; Gallie, R.; Loman, J.; Cook, A.; Ahmadian, R.; Falconer, R.; Lin, B.; Gao, G.; *et al*. Tidal turbine deployment in the Bristol Channel: A case study. *Proc. ICE Energy* **2010**, *163*, 93–105. [CrossRef]
13. Mozafari, A.T.J. Numerical Modeling of Tidal Turbines: Methodology Development and Potential Physical Environmental Effects. Master's Thesis, University of Washington, Seattle, WA, USA, 2010.
14. Masters, I.; Williams, A.; Nick-Croft, T.; Togneri, M.; Edmunds, M.; Zangiabadi, E.; Fairley, I.; Karunarathna, H. A Comparison of Numerical Modelling Techniques for Tidal Stream Turbine Analysis. *Energies* **2015**, *8*, 7833–7853. [CrossRef]
15. Draper, S.; Houlsby, G.; Oldfield, M.; Borthwick, A. Modelling tidal energy extraction in a depth averaged coastal domain. *IET Renew. Power Gener.* **2010**, *4*, 545–554. [CrossRef]
16. Ahmadian, R.; Falconer, R.A. Assessment of array shape of tidal stream turbines on hydro-environmental impacts and available power. *Renew. Energy* **2012**, *44*, 318–327. [CrossRef]
17. Plew, D.R.; Stevens, C.L. Numerical modelling of the effect of turbines on currents in a tidal channel—Tory Channel, New Zealand. *Renew. Energy* **2013**, *57*, 269–282. [CrossRef]
18. Vogel, C.R.; Willden, R.H.J.; Houlsby, G.T. A correction for depth—Averaged simulations of tidal turbine arrays. In Proceedings of the 10th European Wave and Tidal Energy Conference (EWTEC), Aalborg, Denmark, 2–5 September 2013.

19. Funke, S.W.; Farrell, P.E.; Piggott, M.D. Tidal turbine array optimisation using the adjoint approach. *Renew. Energy* **2014**, *63*, 658–673. [CrossRef]
20. Divett, T.; Vennell, R.; Stevens, C. Optimization of multiple turbine arrays in a channel with tidally reversing flow by numerical modelling with adaptive mesh. *Philos. Trans. R. Soc. Lond. A Math. Phys. Eng. Sci.* **2013**, *371*. [CrossRef] [PubMed]
21. Nash, S. Development of an Efficient Dynamically Nested Model for Tidal Hydraulics and Solute Transport. Ph.D. Thesis, College of Engineering & Informatics, National University of Ireland, Galway, Ireland, 2010.
22. Nash, S.; Hartnett, M. Development of a nested coastal circulation model: Boundary error reduction. *Environ. Model. Softw.* **2014**, *53*, 65–80. [CrossRef]
23. Nash, S.; Hartnett, M. Nested circulation modelling of inter-tidal zones: Details of a nesting approach incorporating moving boundaries. *Ocean Dyn.* **2010**, *60*, 1479–1495. [CrossRef]
24. Falconer, R.A. A mathematical model study of the flushing characteristics of a shallow tidal bay. *Proc. Inst. Civil Eng.* **1984**, *77*, 311–332. [CrossRef]
25. Hartnett, M.; Nash, S.; Olbert, I. An integrated approach to trophic assessment of coastal waters incorporating measurement, modelling and water quality classification. *Estuar. Coast. Shelf Sci.* **2012**, *112*, 126–138. [CrossRef]
26. Nash, S.; Hartnett, M.; Dabrowski, T. Modelling phytoplankton dynamics in a complex estuarine system. *Proc. ICE Water Manag.* **2010**, *164*, 35–54. [CrossRef]
27. Nishino, T.; Willden, R.H.J. Two-scale dynamics of flow past a partial cross-stream array of tidal turbines. *J. Fluid Mech.* **2013**, *730*, 220–244. [CrossRef]
28. Houlsby, G.T.; Draper, S.; Oldfield, M.L.G. *Application of Linear Momentum Actuator Disc Theory to Open Channel Flow*; Report No OUEL 2296/08; University of Oxford: Oxford, UK, 2008.
29. Fallon, D.; Hartnett, M.; Olbert, A.; Nash, S. The effects of array configuration on the hydro-environmental impacts of tidal turbines. *Renew. Energy* **2014**, *64*, 10–25. [CrossRef]
30. Sutherland, G.; Foreman, M.; Garrett, C. Tidal current energy assessment for Johnstone Strait, Vancouver Island. *J. Power Energy* **2007**, *221*, 147–157. [CrossRef]
31. Karsten, R.H.; McMillan, J.M.; Lickley, M.J.; Haynes, R.D. Assessment of tidal current energy in the Minas Passage, Bay of Fundy. *Proc. Inst. Mech. Part A J. Power Energy* **2008**, *222*, 493–507. [CrossRef]
32. Olbert, A.I.; Nash, S.; Ragnoli, E.; Hartnett, M. Parameterization of turbulence models using 3DVAR data. In Proceedings of the 11th International Conference on Hydroinformatics, New York, NY, USA, 17–21 August 2014.
33. Mason-Jones, A.; O'Doherty, D.M.; Morris, C.E.; O'Doherty, T. Influence of a velocity profile and support structure on tidal stream turbine performance. *Renew. Energy* **2013**, *52*, 23–30. [CrossRef]
34. Achenbach, E. Influence of surface roughness on the cross-flow around a circular cylinder. *J. Fluid Mech.* **1971**, *46*, 321–335. [CrossRef]
35. Vennell, R. Exceeding the Betz limit with tidal turbines. *Renew. Energy* **2013**, *55*, 277–285. [CrossRef]
36. Stallard, T.; Collings, R.; Feng, T.; Whelan, J. Interactions between tidal turbine wakes: Experimental study of a group of three-bladed rotors. *Philos. Trans. R. Soc. Lond. A Math. Phys. Eng. Sci.* **2013**, *371*. [CrossRef] [PubMed]
37. Lewis, M.J.; Neill, S.P.; Hashemi, M.R.; Reza, M. Realistic wave conditions and their influence on quantifying the tidal stream energy resource. *Appl. Energy* **2014**, *136*, 495–508. [CrossRef]
38. Myers, L.E.; Bahaj, A.S. An experimental investigation simulating flow effects in first generation marine current energy converter arrays. *Renew. Energy* **2012**, *37*, 28–36. [CrossRef]
39. Blackmore, T.; Batten, W.M.J.; Bahaj, A.S. Turbulence generation and its effect in LES approximations of tidal turbines. In Proceedings of the 10th European Wave and Tidal Energy Conference, Aalborg, Denmark, 2–5 September 2013.